AGU PUBLICATIONS

Geophysical Research Letters

RESEARCH LETTER
10.1002/2015GL065553

Key Points:
- The soil thermal properties have a large impact on surface temperature in semiarid regions
- The effect of thermal inertia strongly depends on the atmospheric boundary layer
- Diurnal mean and range of temperature are anticorrelated due to the daytime and nighttime asymmetry

Correspondence to:
S. Aït-Mesbah,
Sonia.Aït-Mesbah@lmd.jussieu.fr

Citation:
Aït-Mesbah, S., J. L. Dufresne, F. Cheruy, and F. Hourdin (2015), The role of thermal inertia in the representation of mean and diurnal range of surface temperature in semiarid and arid regions, *Geophys. Res. Lett.*, *42*, 7572–7580, doi:10.1002/2015GL065553.

Received 27 JUL 2015
Accepted 5 SEP 2015
Accepted article online 11 SEP 2015
Published online 30 SEP 2015

The role of thermal inertia in the representation of mean and diurnal range of surface temperature in semiarid and arid regions

S. Aït-Mesbah[1], J. L. Dufresne[1], F. Cheruy[1], and F. Hourdin[1]

[1]Laboratoire de Météorologie Dynamique. Université Pierre et Marie Curie, Paris, France

Abstract In this article we show the possible role of thermal inertia in the large spread of the simulated surface temperature over arid and semiarid regions among climate models. The surface-atmosphere interactions are investigated based on single-column simulations of the DIurnal land-atmosphere Coupling Experiment and on global simulations. Low values of the surface thermal inertia increase the diurnal temperature range (DTR) and the daytime turbulent heat fluxes. The diurnal response of surface temperature to the thermal inertia is asymmetric between daytime and nighttime, inducing a change in the daily mean surface temperature that can reach several degrees over large areas. This asymmetrical response to thermal inertia is shown to be due to the diurnal contrast of the stability state of the atmospheric boundary layer. Thermal inertia in dry regions plays a critical role on both DTR and surface mean temperature and needs to be carefully represented in land surface models.

1. Introduction

An accurate estimation of the daily mean surface temperature and also of the daily minimum and maximum temperatures is important especially for impact studies concerning health and eventually habitability [*Perkins and Alexander*, 2013; *Sherwood and Huber*, 2010]. However, significant biases persist in state-of-the-art climate models. The bias of air surface temperature in models that participate to the Coupled Model Intercomparison Project Phase 5 (CMIP5) [*Taylor et al.*, 2012] is maximum over regions of high elevation and over the Sahara where it is about 2.5°C [*Flato et al.*, 2013]. Over Sahara, the spread (defined here as 2 times the standard deviation) among models of the seasonal mean temperature is about 4°C for the 24 CMIP5 models considered in our study (see Appendix A). Dry regions are characterized by a large amplitude of the diurnal temperature range (DTR). Over Sahara the DTR is about 14°C, and the spread of its estimate among the 24 CMIP5 models considered here is as large as 6°C. It is unclear whether the model deficiencies originate from land surface or atmospheric models. *Holtslag et al.* [2013] identified the variation of the thermal land surface coupling among the 19 models which participated to GABLS3 as the principal source of excessive cooling during the night. Although the influence of atmospheric processes is generally dominant [*Comer and Best*, 2012], *Santanello et al.* [2013] have shown that the influence of land models is larger in dry conditions than in other conditions.

The aim of this study is to identify the key land surface-atmosphere processes controlling the daily mean and the diurnal cycle of surface temperature in semiarid and arid regions and to provide some guidance to reduce the errors of models in these regions. For doing so, we first use the 1-D case of DIurnal land-atmosphere Coupling Experiment (DICE) [*Best et al.*, 2013; *Poulos et al.*, 2002; *Steeneveld et al.*, 2006; *Svensson et al.*, 2011] and run it with two atmospheric models with very different boundary layer scheme (one has a higher turbulent mixing diurnal contrast), coupled with two land surface models with very different hydrological scheme. The soil thermal inertia appears to be critical and its effect is analyzed in detail. Beyond the DTR, the daily mean temperature is also modified due to the asymmetry of the impact of thermal inertia during daytime and nighttime. Global simulations with fixed sea surface temperature (SST) are then used to extend the DICE results. The range of results obtained for the CMIP5 models is then compared to the range of values we obtained with the different model configurations we use.

The paper is structured as follows. First, the numerical 1-D simulations for the DICE case are briefly presented in section 2. Then differences in the simulated diurnal surface temperature are presented in section 3 and

analyzed in section 4. A discussion follows in section 5. Global simulations are analyzed in section 6 and we conclude in section 7.

2. Numerical Models and Simulations

Two versions of the atmospheric global circulation model LMDZ, LMDZ5A, and LMDZ5B are coupled with two versions of the land surface model ORCHIDEE, ORCHIDEE2, and ORCHIDEE11.

In LMDZ5A [*Hourdin et al.*, 2012], the turbulent transport in the planetary boundary layer is represented as a vertical diffusion where the eddy diffusivity coefficient Kz depends on the local Richardson number [*Laval et al.*, 1981]. A prescribed countergradient of 1 K km^{-1} allows heat transport when the vertical profile of temperature is close to stability [*Deardorff*, 1970]. In LMDZ5B [*Hourdin et al.*, 2013], the planetary boundary scheme uses a combination of the *Yamada* [1983] scheme for small-scale turbulence and of the "thermal plume model" of *Rio and Hourdin* [2008] for the representation of the organized structures of the convective boundary layer [*Rio et al.*, 2013].

For the land surface, the two models share the same scheme for the thermal conduction in the soil but have different hydrological schemes. In ORCHIDEE2 (called ORC2 in the following), a two-layer parameterization is used [*Ducoudré et al.*, 1993]. The upper layer has a varying depth and can appear at the surface after rainfall event to deal with short-time processes and disappear after dry spells [*Manabe*, 1969]. In ORCHIDEE11 (called ORC11 in the following), the vertical water transport is described using the Richard's equation [*de Rosnay et al.*, 2002; *d'Orgeval et al.*, 2008] discretized with 11 layers in a 2 m soil column. The layer thickness increases downward from 1 mm for the top layer to 1 m for the bottom layer [*Campoy et al.*, 2013].

A single-column configuration is first used to simulate the test case DICE (Kansas, latitude 37.65°N, longitude 263.265°E). The simulations cover a period of 3 days starting in the afternoon (19 UTC, 2 P.M. local time) of 23 October and ending on 26 October. The land surface model is initialized with a 10 year spin-up using Water and Global Change data [*Weedon et al.*, 2011] from 1990 to 1998 and Smileyberg site data for the year 1999. The local surface characteristics are 80% of C3 grassland with a Leaf Area Index of 0.4, 20% of bare soil, the soil type is loam, and the surface roughness is 0.01 m.

Four versions of the LMDZ-ORCHIDEE model are then run at global scale in full 3-D configuration for AMIP-type simulations with prescribed SST. The grid has 96 points in latitude, 95 in longitude, and 39 vertical levels.

3. Simulated Surface Temperature for the DICE Case

The temporal evolution of the surface temperature in DICE simulations is represented in the Figure 1a. Observations show a typical diurnal cycle of the semiarid regions with a large DTR, of about 24° during the first day. The models capture the general behavior of surface temperature evolution, especially with the LMDZ5B physics coupled to ORC11. For a given atmospheric model, simulations with ORC2 have a smaller DTR than simulations with ORC11 and the difference can reach 11°C. The difference of surface temperature between ORC2 and ORC11 is much larger during nighttime than during daytime. The nighttime difference is on the order of 5°C with LMDZ5A and it reaches 7°C with LMDZ5B.

Such a sensitivity to land surface model was not anticipated since latent heat flux marginally contributes to the energy budget in DICE dry conditions and because both models share the same thermal conduction scheme. The explanation for this sensitivity lies in the coupling between humidity and thermal inertia.

The time evolution of the temperature under the surface is given by the equation

$$\frac{\partial T}{\partial t} = -\frac{1}{C}\frac{\partial F}{\partial z} \tag{1}$$

where z is the depth and F the conductive heat flux which is given by

$$F = -\lambda \frac{\partial T}{\partial z} \tag{2}$$

where C (J m^{-3} K^{-1}) is the volumetric heat capacity, and λ (W m^{-1} K^{-1}) is the heat conductivity. In the case of vertically homogeneous soil (which is assumed here), it can be shown from equations (1) and (2) using $z' = z \times \sqrt{C/\lambda}$, that the conductive heat flux reads as follows:

$$F = \sqrt{C\lambda}\frac{\partial T}{\partial z'} \tag{3}$$

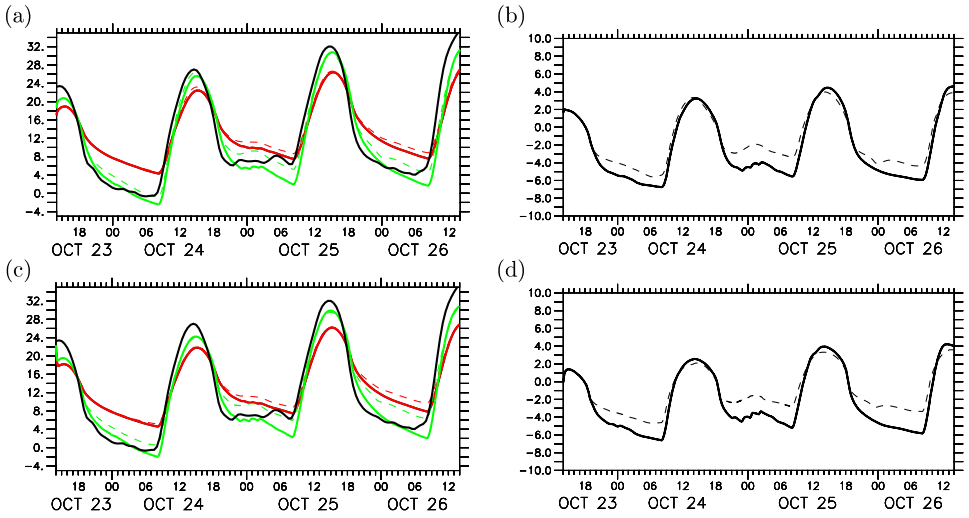

Figure 1. (a) Time evolution of surface temperature for the DICE case. Black line corresponds to observations, red curves corresponds to simulations with ORC2 and green ones to simulations with ORC11. The solid curves correspond to simulations with LMDZ5B atmospheric model and the dotted ones to simulations with LMDZ5A. (b) Differences of surface temperature between ORC11 and ORC2, coupled to LMDZ5A (dotted line), and LMDZ5B (solid line). (c and d) Similar to Figures 1a and 1b but correspond to simulation with imposed ratio of evaporation to potential evaporation $\beta = 0.03$, and imposed thermal inertia: 2190 J m^{-2} K^{-1} s$^{-0.5}$ for red curves and 946 J m^{-2} K^{-1} s$^{-0.5}$ for the green curves (see text).

Hence, the magnitude of temperature fluctuations at the surface depends on the thermal inertia I (J m^{-2} K^{-1} s$^{-0.5}$) with $I = \sqrt{C\lambda}$.

The soil thermal properties λ and C depends on the soil moisture and above all increases with soil water content. The thermal inertia can vary from 600 to 2300 J m^{-2} K$^{-1}s^{-0.5}$ [*Murray and Verhoef*, 2007]. The dependence of thermal inertia to soil moisture is taken into account in ORCHIDEE using the saturation degree of the soil, following *Farouki* [1981]. The difference between ORC2 and ORC11 arises from the difference in the vertical discretization of the two hydrological schemes. ORC2 has only one layer during this dry period and has therefore a constant soil moisture profile over its 2 m depth layer. This leads to a high value of thermal inertia at the surface of 2190 J m^{-2} K^{-1} s$^{-0.5}$. ORC11 has a better hydrological vertical discretization that produces a decreasing soil moisture profile from deeper soil layers to the surface in this case (data not shown). This leads to a lower thermal inertia at the surface of about 946 J m^{-2} K^{-1} s$^{-0.5}$, which is less than half the value using ORC2.

For an imposed oscillation flux of amplitude ΔF at the surface, the DTR is inversely proportional to the thermal inertia, according to DTR= $\Delta F/(I\sqrt{2\pi/\tau})$, where τ is the period of oscillation [*Wang et al.*, 2010]. In our case, the DTR is increased by 2/3 in LMDZ5A and by 3/5 in LMDZ5B when the thermal inertia is divided by more than two. This means that ΔF, and therefore the atmospheric processes are also impacted by a modification of the thermal inertia and attenuate the effect of the thermal inertia on the DTR.

In order to confirm the dominant role of thermal inertia in the difference obtained between ORC2 and ORC11, two additional simulations are performed bypassing the hydrological scheme by prescribing the ratio β of evaporation to potential evaporation to a value adjusted to the DICE case (i.e., $\beta = 0.03$) during the full run. The dependency of soil thermal properties on water content is removed and prescribed to obtain the two different values of thermal inertia obtained with ORC2 and ORC11, which are 2190 and 946 J m^{-2} K^{-1} s$^{-0.5}$, respectively. To do so, the thermal conductivity is prescribed to 1.60 and 0.48 W m^{-1} K^{-1}, respectively, and the thermal capacity is prescribed to 2.70×10^6 and 1.87×10^6 J m^{-3} K^{-1}, respectively. The results presented in the Figures 1c and 1d are very similar to those obtained with the two ORCHIDEE versions (Figures 1a and 1b), confirming the dominant role of thermal inertia in the difference obtained between ORC2 and ORC11.

The simulations show a large asymmetry between the nighttime and the daytime response of the surface temperature to thermal inertia. This asymmetry is larger when using the LMDZ5B atmospheric model. *Kumar et al.* [2014] find a similar asymmetry between the daytime and the nighttime response of the surface

temperature to thermal properties with changes up to 2°–3° for the day minimum surface temperature and minor changes for the day maximum surface temperature. The authors justify this asymmetry by the negative feedback of clouds on the net radiation, and therefore on the surface temperature, during daytime. This explanation, however, does not apply in the present dry and noncloudy case.

4. Simplified Energy Balance Model

To perform a quantitative analysis of the results, we develop an energy balance model at the surface considering the mean value of each variable during daytime and nighttime. This model is based on the hypothesis that regardless of the soil thermal properties, the total energy stored in the soil during daytime is released at the surface during the night. This approximation would be true in a steady state climate with a constant diurnal cycle. In this case, the integrated value of ground heat flux over the full day is zero and reads:

$$\alpha G_d + (1-\alpha) G_n = 0 \tag{4}$$

G_d and G_n are the soil heat fluxes (positive downward) averaged over daytime and nighttime, respectively, and α is the fraction of the daytime (0.36 in the present case). The fraction of daytime is defined as the fraction of day during which the surface heats deeper soil layers ($G > 0$). We have verified that α is independent from the soil thermal inertia used. Note that if the equilibrium hypothesis is not valid, a correction term must be introduced (see Appendix A).

The sum φ_s of net shortwave radiation (SW_{net}) and downward longwave radiation at the surface (LW_{down}) is balanced by sensible (H) and latent (LE) turbulent heat fluxes, upward longwave radiation (LW_{up}), and soil heat flux (G). The flux φ_s is positive when the surface is heated, and all other fluxes are positive when the surface is cooled. The daytime (subscript d) and nighttime (subscript n) energy balances read as follows:

$$\varphi_{sd} = H_d + LE_d + LW_{upd} + G_d \tag{5}$$

$$\varphi_{sn} = H_n + LE_d + LW_{upn} + G_n \tag{6}$$

Deducing G_d and G_n from the equations (6) and (7), and replacing them in the equation (4) lead to the following:

$$\alpha\varphi_{sd} + (1-\alpha)\varphi_{sn} = \alpha(H_d + LE_d + LW_{upd}) + (1-\alpha)(H_n + LE_n + LW_{upn}) \tag{7}$$

The difference of a given variable X between the two simulations with different thermal inertia is defined by $\delta X = X_{I2} - X_{I1}$, where I refers to the thermal inertia. Assuming that the fraction α of daytime does not depend on thermal inertia, the variation of each component of the energy balance with thermal inertia reads as follows:

$$\alpha\left(\delta\varphi_{sd} - \delta H_d - \delta LE_d - \delta LW_{upd}\right) + (1-\alpha)\left(\delta\varphi_{sn} - \delta H_n - \delta LE_n - \delta LW_{upn}\right) = 0 \tag{8}$$

Assuming that these differences are mainly due to the surface temperature change δT_s and defining $X' = \delta X / \delta T_s$ leads to

$$\alpha\left(\varphi'_{sd} - H'_d - LE'_d - LW'_{upd}\right)\delta T_{sd} + (1-\alpha)\left(\varphi'_{sn} - H'_n - LE'_n - LW'_{upn}\right)\delta T_{sn} = 0 \tag{9}$$

To highlight the asymmetry between the daytime and the nighttime response of the surface temperature to thermal inertia, this equation can also be written as follows:

$$\frac{\delta T_{sn}}{\delta T_{sd}} = -\overbrace{\frac{\alpha}{(1-\alpha)}}^{(1)} \overbrace{\frac{\left(\varphi'_{sd} - H'_d - LE'_d - LW'_{upd}\right)}{\left(\varphi'_{sn} - H'_n - LE'_n - LW'_{upn}\right)}}^{(2)} \tag{10}$$

Table 1. Parameter Values Used by the Conceptual Model and Computed From 24 October at 8 h 47 to 26 October 1999 of the DICE Case, Using LMDZ5A and LMDZ5B Atmospheric Models

	φ'_{sd}	φ'_{sn}	LW'_{upd}	LW'_{upn}	H'_d	H'_n	LE'_d	LE'_n	C	D	δT_{sd}	δT_{sn}	$\delta\overline{T_s}$	δDTR
LMDZ5A	0.5	0.5	5.7	5.2	30.1	6.0	4.6	0.8	−1.9	0.5	−1.7	2.2	0.8	6
LMDZ5B	1.2	0.7	6.3	5.1	26.9	0.9	4.6	0.6	−3.5	0.8	−1.6	3.9	1.9	9

5. Role of the Boundary Layer

Equation (10) shows that the ratio between the nighttime and the daytime response of the surface temperature to thermal inertia depends on the length of daytime and on the ratio between the daytime and nighttime sensitivity of atmospheric fluxes to the surface temperature. If the length of daytime is equal to the length of nighttime and if the sensitivity of atmospheric fluxes to the surface temperature is the same during day and night, the response of the surface temperature to thermal inertia is symmetric between day and night. The DTR therefore changes without impacting the mean surface temperature. This is not the case in the present study.

The values of the terms in equation (10) are given in Table 1. Both daytime and nighttime values of φ_s are almost insensitive to a change in thermal inertia. This is mainly because the atmosphere is free of clouds. The daily temperature range is small enough that the sensitivity of the upward longwave radiation to temperature is about the same for both daytime and nighttime ($LW'_{upd} \simeq LW'_{upn}$, see Table 1). In contrast, model results show a large difference between daytime and nighttime sensitivity of both sensible and latent heat fluxes. The sensitivity of turbulent heat fluxes during daytime is 5 to 20 times larger than during nighttime, depending on the atmospheric model. Note, however, that the DICE case being a relatively dry case, the contribution of the latent heat flux is about 6 times lower than the contribution of the sensible heat flux. As a result, the sensitivity φ'_s can be neglected, the sensitivity LW'_{up} can be assumed to be the same during daytime and nighttime, and equation (10) can be written as follows:

$$\frac{\delta T_{sn}}{\delta T_{sd}} = -\frac{\alpha}{(1-\alpha)} \frac{\left(H'_d + LE'_d + LW'_{up}\right)}{\left(H'_n + LE'_n + LW'_{up}\right)} \tag{11}$$

All sensitivities of the fluxes to the temperature are positive. Therefore, if $(H'_d + LE'_d) > (H'_n + LE'_n)$, $|\delta T_{sn}| > |\delta T_{sd}|$. This effect can be attenuated depending on the ratio $\alpha/(1-\alpha)$ between the length of the day and that of the night.

Note that the difference of the DTR is larger than the difference $\delta T_{sd} - \delta T_{sn}$ because the latter is computed with mean values and the DTR is computed with extreme values.

The important role of the surface-atmosphere thermal coupling and the vertical diffusion during the night has already been discussed in *Bosveld et al.* [2014] and in *Sandu et al.* [2013]. The turbulent heat fluxes depend on the stability of the planetary boundary layer. The larger the instability, the higher the sensitivity of turbulent heat fluxes to surface temperature. Because of the solar forcing, the boundary layer is unstable during daytime and a small variation of surface temperature due to soil thermal properties translates into large variations of turbulent heat fluxes. Hence, the sensitivity of surface temperature to thermal inertia is low during daytime. During the night, the total energy stored during the day in the soil is released at the surface. The atmosphere is stable and almost decoupled from the surface, the turbulent heat fluxes remain small, and only the LW_{up} responds to temperature changes. A small change of the ground heat flux translates into large variations of the surface temperature. The sensitivity of the night temperature to thermal inertia is large.

In other words, for a given α, the higher the contrast of the stability of the boundary layer between daytime and nighttime, the larger the asymmetry of the sensitivity of surface temperature to thermal inertia. In the DICE case, α is equal to 0.36, thus reducing these effects by half.

The diurnal contrast of the turbulent heat fluxes also explains the sensitivity differences of the surface temperature to thermal inertia for the two atmospheric models as mentioned in section 3. The LMDZ5A model produces more turbulent mixing during nighttime and slightly less mixing during daytime compared to LMDZ5B (see Table 1). The diurnal contrast of the turbulent fluxes is thus lower in LMDZ5A, leading to a weaker asymmetry of the surface temperature response to the thermal inertia.

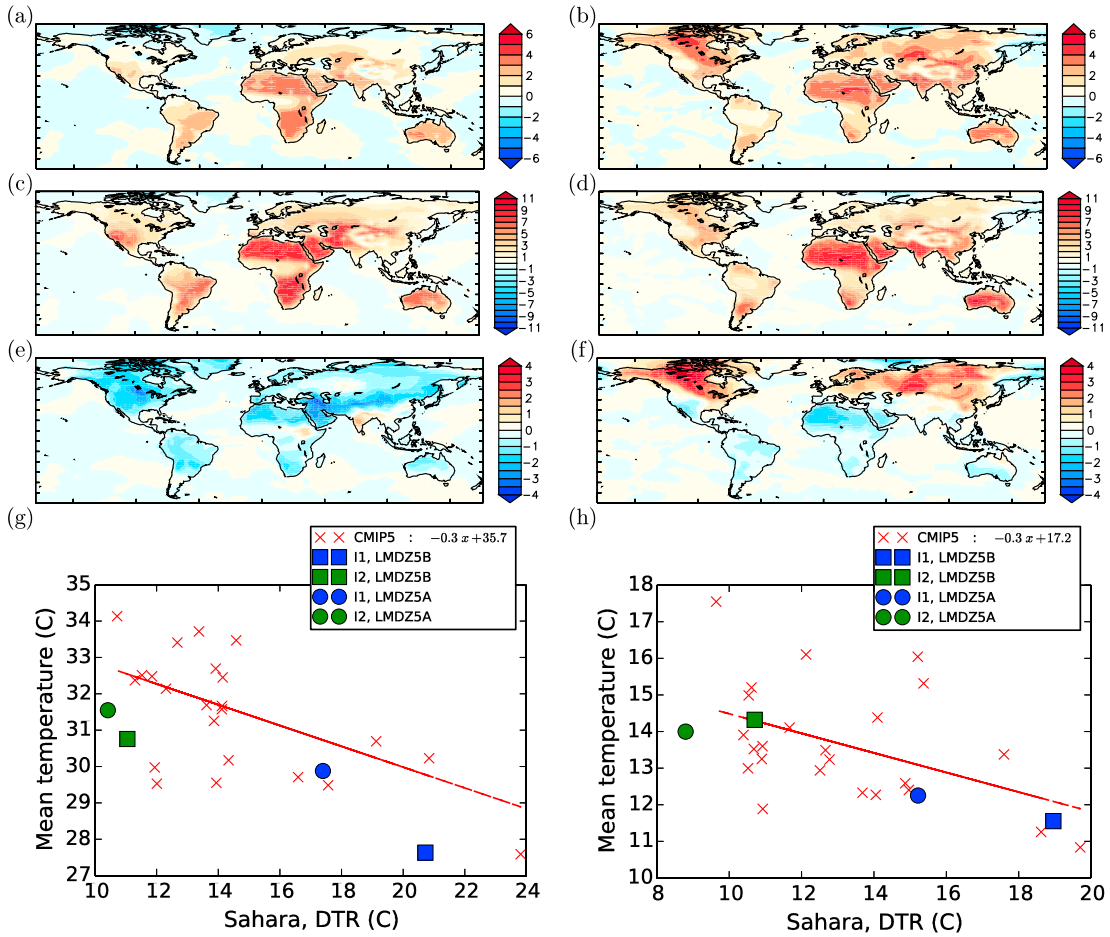

Figure 2. Geographical distribution of the sensitivity of (a and b) mean, (c and d) minimum, and (e and f) maximum day air surface temperatures to a change in thermal inertia from $I1 = 850$ to $I2 = 2400$ J m^{-2} K^{-1} s$^{-0.5}$. (g and h) Scatterplot of the mean temperature versus the DTR over the Sahara (10°W-20°E, 25–30°N) for 24 CMIP5 models (red cross) with the corresponding linear regression line (red line), LMDZ5A (circle) and LMDZ5B (square) coupled to a surface model with a small (blue, $I1 = 850$ J m^{-2} K^{-1} s$^{-0.5}$) and large (green, $I2 = 2400$ J m^{-2} K^{-1} s$^{-0.5}$) thermal inertia. The data are averaged over the June-July-August-September (JJAS) (Figures 2a, 2c, 2e, and 2g) and the December-January-February-March (DJFM) (Figures 2b, 2d, 2e, and 2f) seasons. Note that the scales go from −6 to 6 for the mean surface temperature, from −11 to 11 for the minimum surface temperature, and −4 to 4 for the maximum day surface temperature.

The diurnal asymmetry of the temperature response to thermal inertia leads to a modification of the daily mean temperature: $\overline{T_s} = \alpha T_{sd} + (1-\alpha) T_{sn}$. The impact of the thermal inertia on the mean surface temperature is about 0.8° in LMDZ5A and 1.9° in LMDZ5B (see Table 1). This impact primarily depends on the difference between the daytime and the nighttime sensitivity of the different fluxes to the surface temperature, as deduced from equation (11):

$$\overline{T_s} = \alpha \delta T_{sd} \left(1 - \frac{H'_d + LE'_d + LW'_{up}}{H'_n + LE'_n + LW'_{up}} \right) \tag{12}$$

Note that this conceptual model was also applied on DICE simulations where ORC2 and ORC11 are used. The results are consistent with the results obtained when the β coefficient is prescribed (data not shown) because the contribution of the latent heat flux in this dry case is very low.

6. Extension to Other Dry Regions and Comparison With CMIP5 Models

To evaluate the impact of thermal inertia on the surface temperature diurnal cycle at the global scale, four sensitivity runs have been performed with the two atmospheric models, LMDZ5A and LMDZ5B, coupled to the land surface model ORC11 whose thermal inertia was prescribed with two extreme values (850 and 2400 J m^{-2} K^{-1} s$^{-0.5}$) that span the range of possible values. They correspond to a change of thermal inertia of ±50% around 1600 J m^{-2} K^{-1} s$^{-0.5}$.

Results with LMDZ5B are presented in Figure 2 and show that the sensitivity obtained in the DICE case is representative of arid and semiarid regions. They show a high sensitivity of the surface temperature to thermal inertia over most dry regions. These dry conditions can be permanent (e.g., Sahara, Arabian peninsula) or seasonal (e.g., Sahel, Great Plains in the USA). The daytime surface temperature sensitivity to the thermal inertia is asymmetric. The sensitivity of the minimum surface temperature during nighttime is much higher (8°C over Sahara) than the sensitivity of the maximum temperature during daytime (2°C over Sahara). This asymmetry in the sensitivity of daytime and nighttime temperatures to thermal inertia translates into a sensitivity of a daily mean surface temperature larger than 2°C over many dry regions. An underestimated soil thermal inertia results in an overestimated DTR which in turn lowers the daily mean temperature because of the asymmetric sensitivity. The variation of DTR and mean temperature when changing thermal inertia are anticorrelated.

In order to compare the results obtained with the four LMDZ-OR model configurations and the 24 CMIP5 models, we plot in Figures 2g and 2h the mean temperature as a function of the DTR over Sahara (10°W–20°E, 25–30°N) for JJAS and DJFM, respectively. The anticorrelation between the DTR and the mean temperature we found when changing thermal inertia is also present when modifying the atmospheric physics from LMDZ5A to LMDZ5B and when comparing the whole set of 24 CMIP5 models. The sensitivity of the daily mean surface temperature to thermal inertia due to the asymmetric response of daytime and nighttime temperatures appears to be a more general property.

The LMDZ-OR simulations cover the range of DTR obtained with the CMIP5 models. An uncertainty on thermal inertia of ±50%, which is the example we consider, has an impact on DTR of 7 to 10°C, i.e., of the order of the CMPI5 multimodel spread. The range of thermal inertia we consider may be too large, but these results highlight that thermal inertia is a parameter that is crucial over dry regions and its value need to be carefully estimated in land surface models.

In our simulations DTR is weakly sensitive (<2°C) to the atmospheric model when the soil thermal inertia is large, whereas DTR is more sensitive (≈4°C) when the thermal inertia is small. Conversely, DTR is more sensitive to thermal inertia when the diurnal contrast of the PBL stability is high (LMDZ5B) rather than when this contrast is low (LMDZ5A). Over arid and semiarid regions, both atmospheric and land surface processes interact strongly and it is difficult to quantify independently the relative importance of each of these processes.

7. Conclusion

The soil thermal inertia impacts directly the diurnal temperature range (DTR) with lower thermal inertia inducing higher DTR (and vice versa). But it also impacts the turbulent heat fluxes and this study demonstrates the importance of the diurnal variation of the stability of the atmospheric boundary layer on the sensitivity of surface temperature to thermal inertia. During daytime, when the atmosphere is unstable, changes in soil thermal properties mainly impact turbulent heat fluxes, whereas during nighttime, when the atmosphere is stable, changes in soil thermal properties mainly impact the net longwave radiation flux and the surface temperature.

As a consequence, the response of surface temperature to a change of thermal inertia is asymmetrical with a larger response during the night than during the day. This asymmetry induces a change of the daily mean temperature, and not only a change of the DTR. The asymmetry increases when the diurnal contrast of the stability of the planetary boundary layer increases. This sensitivity to the thermal inertia is large on the global scale and, in particular, over a large fraction of the dry regions. For example, a change of the thermal inertia by ±50% modifies the mean temperature over the Sahara by about 3°C.

This study highlights the importance of a good representation of the dependency of soil thermal properties to both geological properties and soil water content in land surface models. In particular, land surface models should simulate a precise description of the vertical water profile near the surface since only the first few centimeters of the land surface control the thermal inertia and therefore the diurnal cycle of surface temperature.

Appendix A: CMIP5 Models Used

The 24 CMIP5 models used in this study are the following: ACCESS1-0, ACCESS1-3, BNU-ESM, CanAM4, CCSM4, CESM1-CAM5, CMCC-CM, CNRM-CM5, CSIRO-Mk3-6-0, EC-EARTH, FGOALS-s2, GFDL-CM3, GFDL-HIRAM-C180,

GFDL-HIRAM-C360, GISS-E2-R, HadGEM2-A, INMCM4, MIROC5, MPI-ESM-LR, MPI-ESM-MR, MRI-AGCM3-2H, MRI-AGCM3-2S, MRI-CGCM3, and NorESM1-M.

Appendix B: Drift Determination

As shown in Figure 1, the temperature tends to increase from one day to the other, which illustrates the fact that equilibrium is not reached. The hypothesis stated in the equation (4) is not valid. A corrective term is therefore introduced, and the equation (8) should be written as follows:

$$\alpha\delta G_d + (1-\alpha)\delta G_n = \alpha(\delta\varphi_{\mathrm{sd}} - \delta H_d - \delta \mathrm{LE}_d - \delta \mathrm{LW}_{\mathrm{upd}}) + (1-\alpha)(\delta\varphi_{\mathrm{sn}} - \delta H_n - \delta \mathrm{LE}_n - \delta \mathrm{LW}_{\mathrm{upn}}) \tag{B1}$$

Hence, the ratio $\left(\delta T_{\mathrm{sn}}/\delta T_{\mathrm{sd}}\right)_{\mathrm{drift}}$ representing the ratio of the sensitivity of nighttime surface temperature to the daytime surface temperature when the equilibrium is not reached is equal to

$$\left(\frac{\delta T_{\mathrm{sn}}}{\delta T_{\mathrm{sd}}}\right)_{\mathrm{drift}} = \overbrace{-\frac{\alpha}{(1-\alpha)}\frac{(\varphi'_{\mathrm{sd}} - H'_d - \mathrm{LE}'_d - \mathrm{LW}'_{\mathrm{upd}})}{\left(\varphi'_{\mathrm{sn}} - H'_n - \mathrm{LE}'_n - \mathrm{LW}'_{\mathrm{upn}}\right)}}^{C} + \overbrace{\frac{1}{(1-\alpha)}\frac{\alpha\delta G_d + (1-\alpha)\delta G_n}{\delta T_{\mathrm{sd}}\left(\varphi'_{\mathrm{sn}} - H'_n - \mathrm{LE}'_n - \mathrm{LW}'_{\mathrm{upn}}\right)}}^{D} \tag{B2}$$

where C is the value at equilibrium and D is the value due to the drift (see Table 1 for the value of each term). In the text, the values of δT_{sd} and δT_{sn} are defined as values at the equilibrium while the equilibrium is not reached. Since the value due to the drift (D) is low compared to the value at equilibrium (C) (see Table 1), the performed analysis does not qualitatively change.

Acknowledgments

This research was supported by the European Commission's Seventh Framework Programme EMBRACE project (grant 282672). To analyze the CMIP5 data, this study benefited from the IPSL Prodiguer-Ciclad facility which is supported by CNRS, UPMC, Labex L-IPSL which is funded by the ANR (grant ANR-10-LABX-0018) and by the European FP7 IS-ENES2 project (grant 312979). We acknowledge Martin Best and Adrian Lock from the Met Office for providing us the large-scale forcing for the 1-D DICE case, and Marie Pierre Lefebvre from Météo-France/IPSL for helping us to set up this 1-D case. Both the data and input files necessary to reproduce this study are available from the authors upon request (Sonia.Ait-Mesbah@lmd.jussieu.fr).

The Editor thanks Albert Holtslag and an anonymous reviewer for their assistance in evaluating this paper.

References

Best, M., A. Lock, J. Santanello, G. Svensson, and B. Holtslag (2013), A new community experiment to understand land-atmosphere coupling processes, *GEWEX News*, *23*, 3–5.

Bosveld, F., et al. (2014), The third GABLS intercomparison case for evaluation studies of boundary-layer models. Part B: Results and process understanding, *Boundary Layer Meteorol.*, *152*(2), 157–187, doi:10.1007/s10546-014-9919-1.

Campoy, A., A. Ducharne, F. Cheruy, F. Hourdin, J. Polcher, and J. C. Dupont (2013), Response of land surface fluxes and precipitation to different soil bottom hydrological conditions in a general circulation model, *J. Geophys. Res. Atmos.*, *118*, 10,725–10,739, doi:10.1002/jgrd.50627.

Comer, R. E., and M. J. Best (2012), Revisiting GLACE: Understanding the role of the land surface in land-atmosphere coupling, *J. Hydrometeorol.*, *13*(6), 1704–1718, doi:10.1175/JHM-D-11-0146.1.

de Rosnay, P., J. Polcher, M. Bruen, and K. Laval (2002), Impact of a physically based soil water flow and soil-plant interaction representation for modeling large-scale land surface processes, *J. Geophys. Res.*, *107*(D11), 4118, doi:10.1029/2001JD000634.

Deardorff, J. W. (1970), Convective velocity and temperature scales for the unstable planetary boundary layer and for Rayleigh convection, *J. Atmos. Sci.*, *27*(8), 1211–1213, doi:10.1175/1520-0469(1970)027(1211:CVATSF)2.0.CO;2.

d'Orgeval, T., J. Polcher, and P. de Rosnay (2008), Sensitivity of the West African hydrological cycle in ORCHIDEE to infiltration processes, *Hydrol. Earth Syst. Sci.*, *12*(6), 1387–1401, doi:10.5194/hess-12-1387-2008.

Ducoudré, N. I., K. Laval, and A. Perrier (1993), SECHIBA, a new set of parameterizations of the hydrologic exchanges at the land-atmosphere interface within the LMD atmospheric general circulation model, *J. Clim.*, *6*(2), 248–273, doi:10.1175/1520-0442(1993)006(0248:SANSOP)2.0.CO;2.

Farouki, O. T. (1981), The thermal properties of soils in cold regions, *Cold Reg. Sci. Technol.*, *5*(1), 67–75, doi:10.1016/0165-232X(81)90041-0.

Flato, G., et al. (2013), Evaluation of climate models, in *Climate Change 2013: The Physical Scientific Basis. Contribution of Working Group I to the Fifth Assessment Report of the Intergovernmental Panel on Climate Change*, edited by T. Stocker et al., chap. 9, pp. 741–866, Cambridge Univ. Press, Cambridge, U. K., and New York, doi:10.1017/CBO9781107415324.020.

Holtslag, A. A. M., et al. (2013), Stable atmospheric boundary layers and diurnal cycles: Challenges for weather and climate models, *Bull. Am. Meteorol. Soc.*, *94*, 1691–1706.

Hourdin, F., et al. (2012), Impact of the LMDZ atmospheric grid configuration on the climate and sensitivity of the IPSL-CM5a coupled model, *Clim. Dyn.*, *40*(9–10), 2167–2192, doi:10.1007/s00382-012-1411-3.

Hourdin, F., et al. (2013), LMDZ5b: The atmospheric component of the IPSL climate model with revisited parameterizations for clouds and convection, *Clim. Dyn.*, *40*(9–10), 2193–2222, doi:10.1007/s00382-012-1343-y.

Kumar, P., R. Podzun, S. Hagemann, and D. Jacob (2014), Impact of modified soil thermal characteristic on the simulated monsoon climate over south Asia, *J. Earth Syst. Sci.*, *123*(1), 151–160, doi:10.1007/s12040-013-0381-0.

Laval, K., R. Sadourny, and Y. Serafini (1981), Land surface processes in a simplified general circulation model, *Geophys. Astrophys. Fluid Dyn.*, *17*(1), 129–150, doi:10.1080/03091928108243677.

Manabe, S. (1969), Climate and the ocean circulation1, *Mon. Weather Rev.*, *97*(11), 739–774, doi:10.1175/1520-0493(1969)097(0739:CATOC)2.3.CO;2.

Murray, T., and A. Verhoef (2007), Moving towards a more mechanistic approach in the determination of soil heat flux from remote measurements: I. A universal approach to calculate thermal inertia, *Agric. For. Meteorol.*, *147*(1–2), 80–87, doi:10.1016/j.agrformet.2007.07.004.

Perkins, S. E., and L. V. Alexander (2013), On the measurement of heat waves, *J. Clim.*, *26*, 4500–4517, doi:10.1175/JCLI-D-12-00383.1.

Poulos, G. S., et al. (2002), Cases-99: A comprehensive investigation of the stable nocturnal boundary layer, *Bull. Am. Meteorol. Soc.*, *83*, 555–581.

Rio, C., and F. Hourdin (2008), A thermal plume model for the convective boundary layer: Representation of cumulus clouds, *J. Atmos. Sci.*, *65*(2), 407–425, doi:10.1175/2007JAS2256.1.

Rio, C., et al. (2013), Control of deep convection by sub-cloud lifting processes: The ALP closure in the LMDZ5b general circulation model, *Clim. Dyn.*, *40*(9–10), 2271–2292, doi:10.1007/s00382-012-1506-x.

Sandu, I., A. Beljaars, P. Bechtold, T. Mauritsen, and G. Balsamo (2013), Why is it so difficult to represent stably stratified conditions in numerical weather prediction (NWP) models?, *J. Adv. Model. Earth Syst.*, *5*(2), 117–133, doi:10.1002/jame.20013.

Santanello, J. A., C. D. Peters-Lidard, A. Kennedy, and S. V. Kumar (2013), Diagnosing the nature of land-atmosphere coupling: A case study of dry/wet extremes in the U.S. Southern Great Plains, *J. Hydrometeorol.*, *14*(1), 3–24, doi:10.1175/JHM-D-12-023.1.

Sherwood, S. C., and M. Huber (2010), An adaptability limit to climate change due to heat stress, *Proc. Natl. Acad. Sci. U.S.A.*, *107*(21), 9552–9555, doi:10.1073/pnas.0913352107.

Steeneveld, G. J., B. J. H. van de Wiel, and A. A. M. Holtslag (2006), Modeling the evolution of the atmospheric boundary layer coupled to the land surface for three contrasting nights in CASES-99, *J. Atmos. Sci.*, *63*(3), 920–935, doi:10.1175/JAS3654.1.

Svensson, G., A. Holtslag, V. Kumar, T. Mauritsen, G. Steeneveld, W. Angevine, E. Bazile, A. Beljaars, E. d. Bruijn, and A. Cheng (2011), Evaluation of the diurnal cycle in the atmospheric boundary layer over land as represented by a variety of single-column models: The second GABLS experiment, *Boundary Layer Meteorol.*, *140*(2), 177–206.

Taylor, K. E., R. J. Stouffer, and G. A. Meehl (2012), An overview of CMIP5 and the experiment design, *Bull. Am. Meteorol. Soc.*, *93*(4), 485–498, doi:10.1175/BAMS-D-11-00094.1.

Wang, J., R. L. Bras, G. Sivandran, and R. G. Knox (2010), A simple method for the estimation of thermal inertia, *Geophys. Res. Lett.*, *37*, L05404, doi:10.1029/2009GL041851.

Weedon, G. P., S. Gomes, P. Viterbo, W. J. Shuttleworth, E. Blyth, H. Österle, J. C. Adam, N. Bellouin, O. Boucher, and M. Best (2011), Creation of the WATCH forcing data and its use to assess global and regional reference crop evaporation over land during the twentieth century, *J. Hydrometeorol.*, *12*(5), 823–848, doi:10.1175/2011JHM1369.1.

Yamada, T. (1983), Simulations of nocturnal drainage flows by a q2l turbulence closure model, *J. Atmos. Sci.*, *40*(1), 91–106, doi:10.1175/1520-0469(1983)040(0091:SONDFB)2.0.CO;2.